Creep-Fatigue Behaviour of Thick Wall Notched Hollow Cylinders

S. Krolop and R. Stegmeyer
Staatliche Materialpruefungsanstalt (MPA)
University of Stuttgart

Third International Conference on Biaxial/Multiaxial Fatigue
April 3-6 1989 Stuttgart FRG

1 INTRODUCTION

During the non-steady operation of components subject to thermal loads created during start-up and run-down procedures, temperature-induced strains of an essentially multiaxial nature occur as the result of non-constant temperatures. In comparison with these strains, the influence of mechanical loads from, for example, internal pressure or centrifugal force, are secondary. The service life of components of this kind is, therefore, essentially determined by thermally induced strains.

At the MPA-Stuttgart for a considerable time, detailed studies have been conducted on the low-cycle-fatigue areas that suffer strain amplitudes beyond the elastic limit. These studies have been concerned with major influential variables and inter-relationships such as cycle time and cycle form, surface properties, notches, temperature, and hold times. All these experiments were carried out on small test rods with mechanically applied strains at constant temperature. Temperature gradients were avoided in the specimens. The application of results obtained with small specimens to large components is, however, always subject to uncertainty as to whether the adopted procedure is justified. In order to clarify this question, experiments were carried out with thick-wall hollow cylinders which were subjected to alternating temperatures including hold times. Circumferential grooves were used to provide a general increase in local strains.

The tests with large-scale specimens constitute the consistant continuation of

tests made earlier at the MPA Stuttgart in the low-cycle-fatigue sector. Figure 1 shows a schematic summary of studies conducted up to the present time.

These large-scale specimen tests run concurrent with numerical calculations according to the finite element (FE) method. They were to provide a deeper insight into the deformation sequences during alternating plastification in conjunction with creep.

To start, the material-mechanical basic features for the time-independent elastoplastic deformation behaviour during cyclic loads and the time-dependent creep problems are discussed in a special section.

This is followed by the discussion of the various theoretical formulations for inelastic material behaviour presented in the preceding section using different principle investigations. The results obtained with the FE method are compared for verification with measuring results prior to transplanting the calculations to realistic tests on the largescale specimens.

2 DEFORMATION BEHAVIOUR UNDER PLASTIC STRAIN

When using materials at increased temperature, inelastic deformations can be frequently expected. In this context, we differentiate between time-independent plastic deformation and time-dependent creep.

2.1 Time-independent deformation behaviour

In practical applications, irreversible deformations frequently occur by repeating load cycles, so that, in addition to an overelastic deformation in the same direction, the overelastic alternating deformation is of primary interest.

In order to be able to describe the elastoplastic deformation behaviour generally, we need, in addition to the Hooke's law which expresses the elastic proportion of strain by the stresses, the following postulates:

- the yield condition, which decides on the onset of plastic yield,

- the flow rule, which specifies the direction of plastic flow,

- the hardening rule, which describes the increase of deformation resistance as a function of plastic deformation.

The yield condition is given by the selection of an appropriate plasticity hypertheses, e.g. the von Mises yield criterion. This reduces the multiaxial stress condition to an equivalent uniaxial stress condition with the equivalent stress σ_e .

The flow rule is associated with the yield condition. It links the plastic strain proportion with the stress deviator. On the basis of the flow theory usually applied, we must, in order to obtain the whole strain components, integrate over the entire load path.

The hardening rule plays an important part in the elastoplastic alternate load, since it specifies the point at which plastification occurs within the cycle after a reversal of the load. In doing so, a material softening or hardening with a change of the technological characteristics (yield limit R_e, ultimate tensile stress R_m) per load cycle may be overlapped in the model. Two models are used as hardening rules in the plasticity theory, which are to describe the characteristic of isotropic and kinematic hardening. The two models are compared by way of example of the uniaxial alternating compression-tension tests with constant strain amplitude in Figure 2. The simplified bilinear representation of the alternating behaviour shows with isotropic hardening, that, after elastic loading or unloading, yield occurs whenever the current stress has reached the maximum value from a preceding load in a reversed direction. In doing so, the isotropic hardening model assumes an increasing elastic range, until in the limit status, the behaviour would be completely elastic. In contrast, the kinematic model shows that the elastic range for each reversal is equal to twice the apparent limit of elasticity and that it remains

constant.

Similar to the yield limit in the 1-dimensional case, the existence of a yield surface is assumed for the general 3-dimensional case. Reduced to a 2-dimensional stress condition, the boundary for elastic material behaviour is given by an ellipse via the von Mises yield criterium. Based on this prerequisite, isotropic hardening means that the apparent yield surface expands to its origin maintaining its form and direction, Figure 3a, while for the kinematic hardening model, which keeps the elastic limit constant, the surface remains unchanged but is subject to a translation with its shift represented by the vector $\{\alpha\}$, Figure 3b.

The actual material behaviour, however, will not accurately follow one of these two models. A refined method, for this reason, means a mixed hardening rule where the translation as well as an expansion of the yield surface is assumed, Figure 4; practical applications, however, show that for cyclic loading, yielding is sufficiently described by the kinematic model.

2.2 Time-dependent Creep

The basic understanding for this is obtained by experiments with uniaxial isothermal model tests under constant load.

For an engineering assessment of creep phenomena, a constitutive connection between the change of strain during time and variable stress at different temperatures is needed. In developing this type of a creep law, two options are available:

- the mechanical behaviour of the material explicitly depends only on the current deformation status,

- the mechanical behaviour depends on the previous history of deformation.

The formulation of a mathematical model on the basis of the first case allows

the consistant separation between the plastic and the creep deformations and constitutes the basis for the following numerical calculations, whereas in the second case, a coupling of both deformation processes is generally assumed.

The most simple mathematical relationship to describe creeping is given by the Bailey-Norton law:

$$\varepsilon_c = A\sigma^n t^m$$

In this equation A,m,n are material constants and dependent of temperature, in which case n states the degree of nonlinearity between stresses and strains.

The differentiation of this equation with respect to time supplies the strain rate for variable stresses:

$$\dot{\varepsilon}_c = \frac{d\varepsilon_c}{dt} = A\sigma^n m t^{m-1}$$

As a result of the time-dependent reference, this relationship constitutes a time-hardening solution, i.e., the relevant creep strain rate is specified by the stress, time and by temperature using the constants.

An additional formulation of creep strain rate is obtained if one eliminates time from the preceding equation. If the creep law is solved for time, and by placing the expression obtained into the above equation, a relationship is found for the creep strain rate which is independent of time (strain hardening theory):

$$\dot{\varepsilon}_c = A^{1/m} m \sigma^{n/m} (\varepsilon_c)^{(m-1)/m}$$

The application of the differing hardening theories is shown in Figure 5 and 6, by determining creep strain for various stress intervals and in conjunction with the associated creep curves. Figure 5 shows the increase of creep strain on the basis of the time hardening theory. Initially, we are moving on the original creep curve for σ_3= const. If the stress is increased from σ_3 to σ_4 at any point (point A on the σ_3 -curve), we follow the course of the σ_4 -curve as of this point. The resulting strain accumulation up to the new stress change is

obtained by shifting the σ_4 -curve parallel from A' to A. Similarly, we can proceed at points B and C to σ_2 or σ_1 respectivly for additional stress changes.

Whereas time is kept constant during the time hardening theory at the time of transition from one creep curve to another, the creep remains constant with the strain hardening theory, Fig. 6.

The described hardening theories allow the calculation of the creep strain for stress changes in the same direction; in contrast thereto it is not possible without appropriate auxiliary rules to register the effect of a stress reversal. The principal procedure in applying such auxiliary rules is explained by way of example in the strain hardening model in Figure 7.

Initially, Fig. 7a shows the assumed stress history, Fig. 7b the associated creep curves. For the sake of simplification, it is assumed that the creep curves under compression are the mirror image of the curves for tension. Creeping starts with σ_3 and the creep strain ε_1 is accumulated. When shifting to stress $-\sigma_1$, it is assumed that the hardening achieved previously under tension is extinguished and creep under compression starts anew, i.e., the creep curve for $-\sigma_1$ corresponds to a nonprehardened material. When changing to a new positive stress σ_2 (t_2), the overall creep strain achieved $\varepsilon_1 - \varepsilon_2$ remains positive as long as the creep strain generated under compression is smaller than the creep achieved previously under tension. Further creep behaviour is then described as of value $\varepsilon_1 - \varepsilon_2$ by the σ_2 -curve, Fig. 7c. In contrast, we start at creep value zero on the σ_2-curve if $\varepsilon_2 > \varepsilon_1$ because the hardening previously built up under σ_3 was totally eliminated. In case that ε_3 was larger mathematically than the creep strain ε_2 accumulated at $-\sigma_1$, the hardening starts at a new compression on the relevant creep curve from the very beginning.

3 NUMERICAL CALCULATIONS

The program system PERMAS /1/ was available for calculations. This program is appropriate for the solution of plastic material problems as well as of creep processes. It was already used successfully with previous elastoplastic calculations and is now to be used in combination with creep or relaxation processes.

First it had to be clarified how well material-mechanical deformation processes can be described with cyclic plastification and creeping by the finite element (FE) code. For this reason, the load cycle of a typical, uniaxial fatigue test as used to determine the incipient crack load cycle was recalculated. Figure 8 shows the type of test specimen which could be idealized with 9-noded axi-symmetric ring elements. With a test temperature of 530 °C and the strain controlled load specification, the subsequent hold time meant a relaxation of the tensile test bar. In particular, this was to clarify if relaxation processes can be imitated satisfactorily by a creep calculation.

A heat resistance 1% Cr-steel (28 CrMoNiV 49) which softened in cycles formed the basis. Cyclic uniaxial stress-strain curves were available for the material named for different test temperatures between room temperature and 530 °C, while the selection of the creep curves was limited to 530 °C. In order to implement into the FE code, the uniaxial stress-strain curves and the creep curves were approximated by polynomes of a higher order; required intermediate values could be determined by linear interpolation.

The hysteresis loops found by assuming isotropic and kinematic material hardening are compared in Figure 9. The strain amplitude was specified with 3.5 0/00. Since the program accurately follows the yield curve on a calculation basis, a comparison with the measurement can be ignored. The courses obtained confirm the behaviour discussed in the preceding chapter, namely that for isotropic hardening, the elastic strain proportion increases while the kinematic hardening model maintains the elastic limit constant.

In order to check the relaxation behaviour, the same FE model was used to apply a strain controlled load from a stress-free original condition to a tensile load of 360 N/mm^2, and with a remaining constant specimen strain, a hold time of 20 minutes was assumed. Since, according to the theory used here, plastification and creep may be viewed as independent processes, it does not make any difference in which way (purely elastic or elastoplastic) the original condition is used. In order to be able to simulate the relaxing of the test bar, the holding time was subdivided into time increments of half a minute and it was assumed that within time interval, creep sets in at the currently prevalent stress within the component.

The decrease of stress over time in the tensile test bar in accordance with the strain hardening theory and the time hardening theory is shown in Figure 10. Since the difference of both theories is procedural and not phenomenological, both curves are similar, but relaxation is greater in accordance with the time hardening theory.

In comparison with the measured curve which was taken from the test protocol of the start-up cycle of a fatigue test with hold time, stress decreases faster on a calculation basis, however, the strain hardening gets closer to the test. The difference between the calculation on the basis of the strain hardening theory and the experiment arises actually within the first minute, while both curves thereafter almost run parallel. It may be assumed that the mathematical formulation of the creep curves do not represent primary creep accurately enough.

In contrast to the calculations for the small-scale specimens, where a mechanically induced load was effective, the large-scale specimen was subjected to alternating temperatures which were based on the current temperature course of a turbine shaft. Figure 11 shows the type of test specimen and its main dimensions.

In order to obtain the temperature course shown in Figure 12, the specimen was inductively heated from outside to 530 °C. Depending on the rate of heating, a more or less steep gradient could be obtained. This gradient can be increased by simultaneously cooling the inner wall. Once the maximum temperature is reached, a steady state is established, while retaining the inner/outer temperature difference. After the inner cooling is switched off, temperature equalization takes place at 530 °C. Subsequent external cooling produces an inverted temperature gradient. Detailed explanation on the performance of the test may be taken from /2/.

The calculations for the large-scale models were carried out in two separate stages. In the first calculation, the transient temperature field was calculated, using the temperature measured at the inner and outer surface of the specimen. The temperature calculated for each node was then multiplied by the associated coefficient of thermal expansion and incorporated into the elastoplastic calculation as initial strain. It was assumed that the model was free

of internal stress at the beginning of the calculation. Both calculations were based on the same number of elements which were of the same type as in the foregoing calculations (axisymmetric ring elements). With the exception of the modulus of elasticity for which a mean value was used in the computations all the material properties were specified as a function of temperature and strain respectively. Due to the cyclic temperatures the elastoplastic calculation followed the kinematic hardening rule.

Figure 13 shows exemplary stress and strain courses in the notched bottom of the large-scale specimen for a temperature cycle without holding time. Since the calculation is based on cyclic yield curves at half the number of cycles required for an incipient crack ($N/N_I=0.5$), the strains measured for $N/N_I=0.5$ were also used for the comparison. The correlation can be considered to be adequate.

The cyclic thermal loading causes in the notched bottom of the large-scale specimen incipient cracking. With knowledge of the strain range the number of cycles up to which incipient cracking occurs can be estimated from the crack initiation curves of isothermal laboratory experiments on round specimens subjected to cyclic uniaxial load at 530 °C, Figure 14.

As the strain range from equivalent and longitudional strain mathematically differ only slightly (see Fig. 13) theoretically both strain values yield about 1300 temperature cycles up to incipient cracking. The crack initiation curve derived from a test series with large-scale specimens on basis of the experimentally reproducable longitudional strain shows, that incipient cracking occurs sooner.

The submitted evaluation makes not evident which strain range governs the incipient cracking behaviour. For this reason the stress range was selected to represent the crack initiation curve instead of the strain range. To confirm the result on the basis of the strain range, the required stress range (see Fig. 13) has to be taken from the equivalent stress.

A hold time after each temperature cycle at 530 °C causes always a relaxation in the same direction. The effect of a 120 minutes lasting hold time on the stresses in the notched bottom of the large-scale specimen is shown in Fi-

gure 16. The calculation is based on the strain hardening theory. The reduction in stress at the end of the hold time approximately amounts to 10 N/mm^2. It is assumed that repeated relaxation will not influence incipient cracking. In the meanwhile this assumption has been verified by a further experiment.

4 SUMMARY

In order to study the incipient crack behaviour at alternating temperatures on assembly-part components, thick-walled hollow cylinders with circumferential notches were selected as test specimens, which were scaled according to a turbine shaft. Alternating temperatures with and without hold times generated incipient cracks in the large-scale specimens.

Elastoplastic finite element calculations concurrent with the test provided information on the deformation behaviour of large-scale specimens. By applying the kinematic hardening rule, a fine agreement between measured and calculated strains was obtained.

The assessment of the incipient crack behaviour for tests without hold times with an incipient crack characteristic registered on laboratory tests resulted in an overestimation of the number of the temperature changes up to the onset of cracking.

Hold times under constant strain which result in relaxation of the stress in uniaxial laboratory tests could be satisfactorily imitated with the strain hardening theory.

A constant temperature of 530 °C over 120 minutes after a preceding temperature cycle generates only minor stress changes in the large-scale specimen.

4 LITERATURE

/1/ PERMAS III/1 - Material Non-Linearities
User's Reference Manual,
INTES Publication No. 207, Rev. D Stuttgart

/2/ Stegmeyer, R.: The Design and Operation of a Test Facility for Temperature Cycling of Large Specimens, Biaxial and Multiaxial Fatigue, EGF3 (Edited by M. W. Brown and K. J. Miller), 1988, Mech. Eng. Pub., London

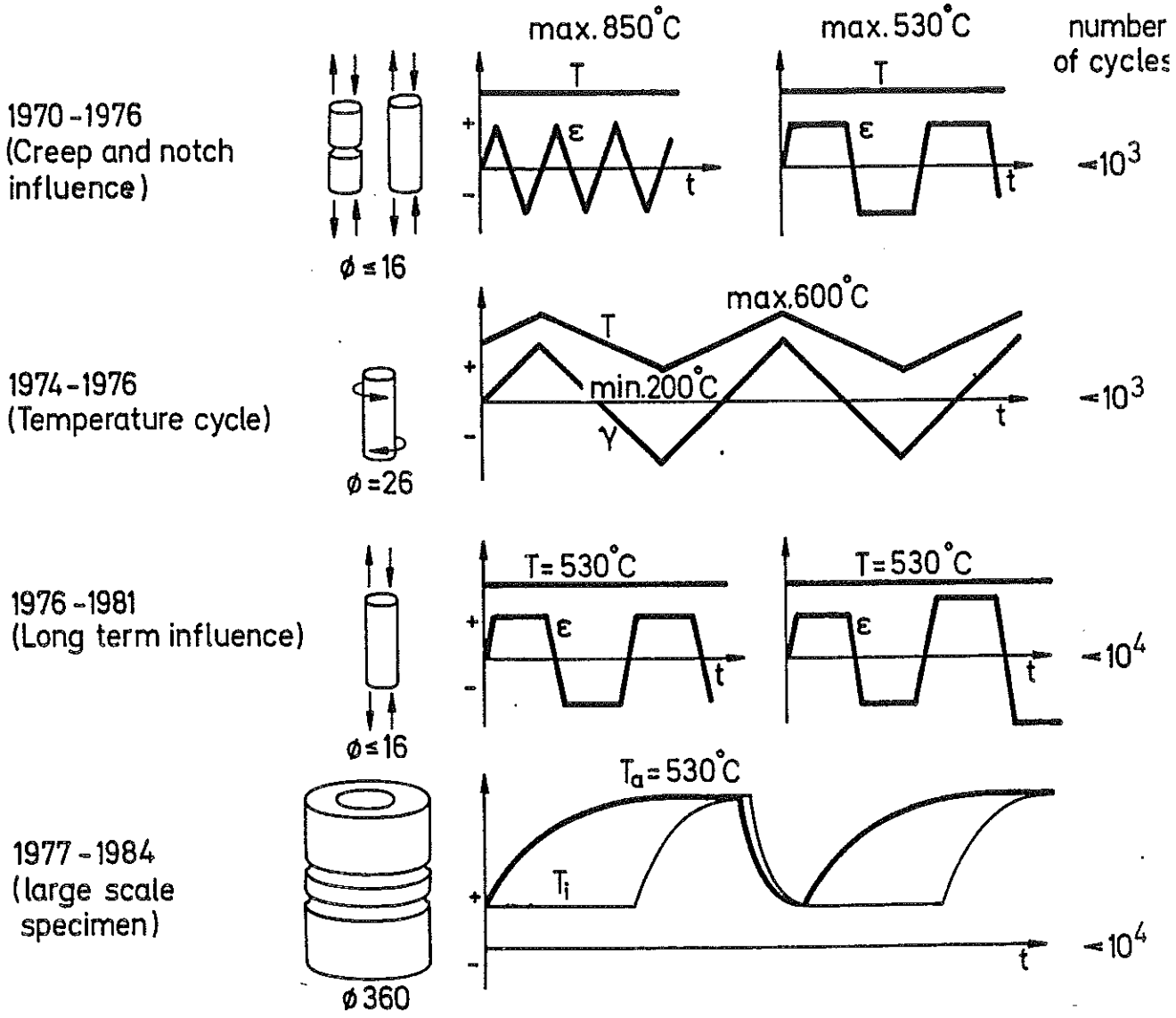

Fig. 1: Schematic summary of studies conducted up to the present time at the MPA

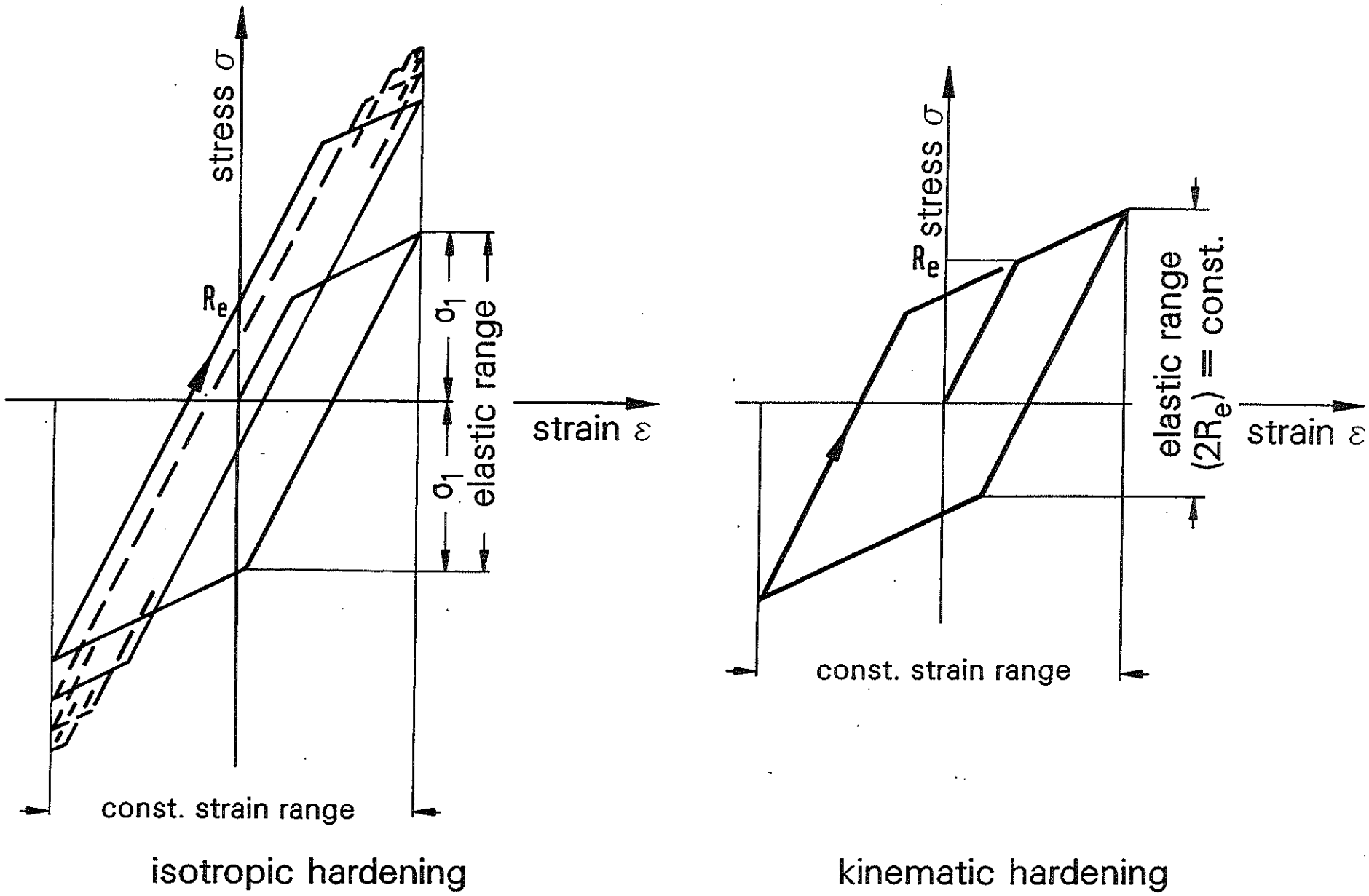

Fig. 2: Schematic stress-strain behaviour for uniaxial cyclic loading by isotropic and kinematic hardening

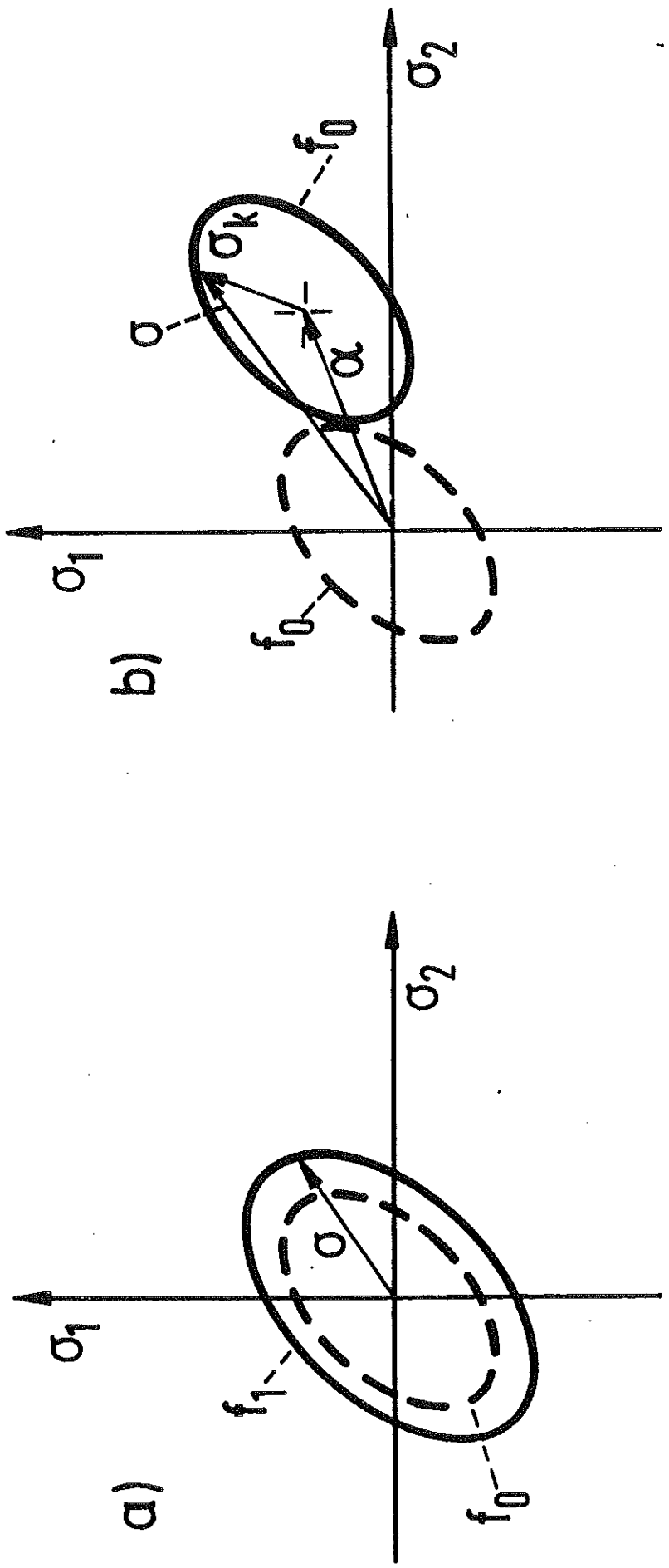

Fig. 3: Schematic description of a) isotropic and b) kinematic hardening in two-dimensional stress space

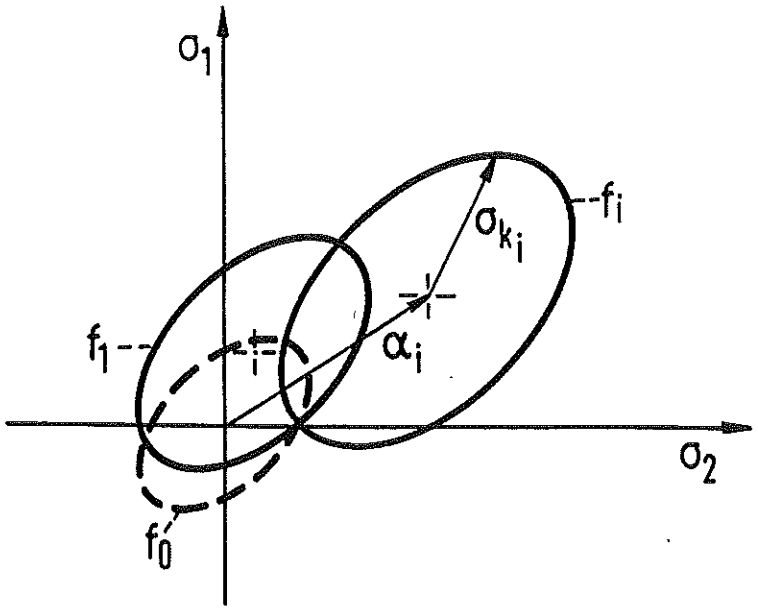

Fig. 4: Mixed hardening model

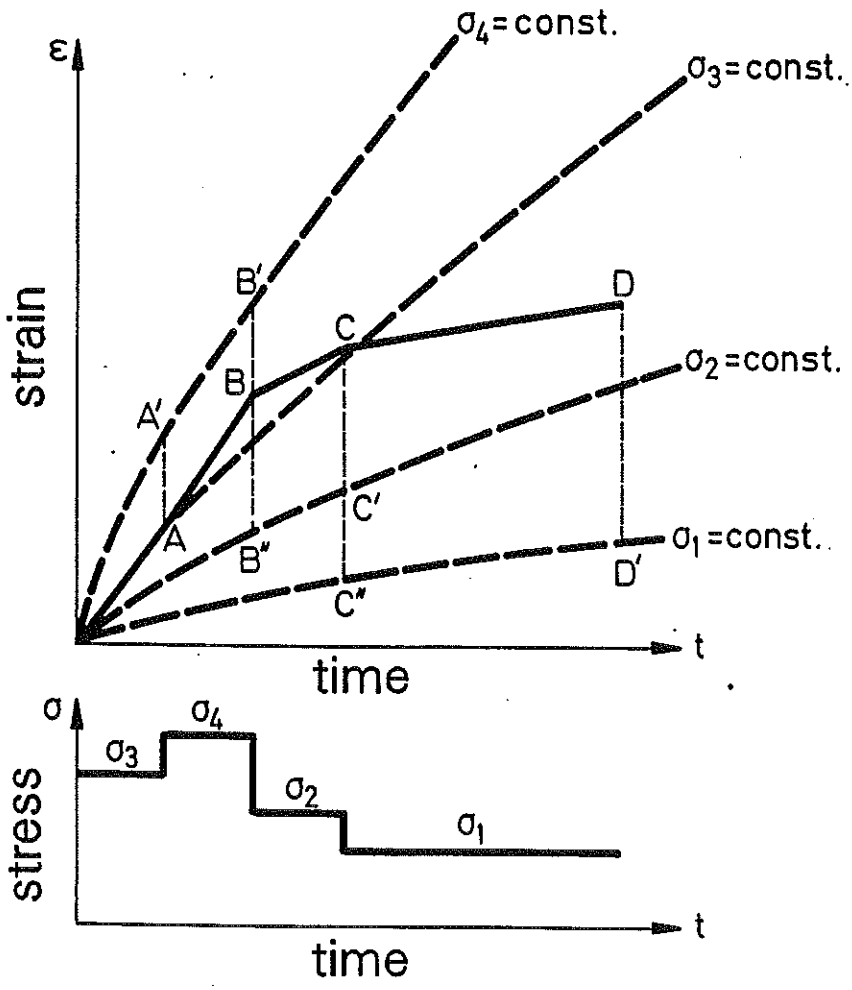

Fig. 5: Creep strain history (time hardening theory)

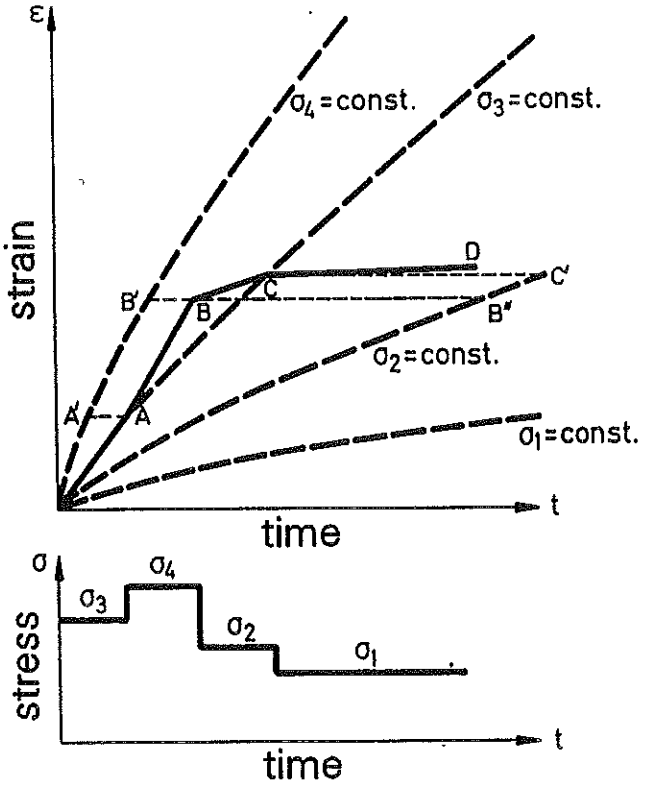

Fig. 6: Creep strain history (strain hardening theory)

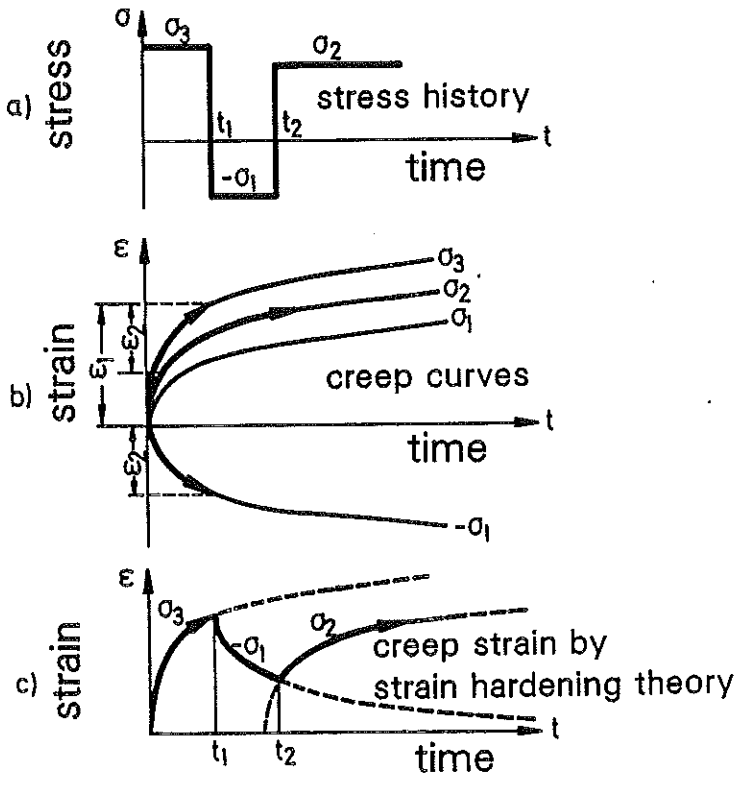

Fig. 7: Presumed creep response when stress reversals are involved

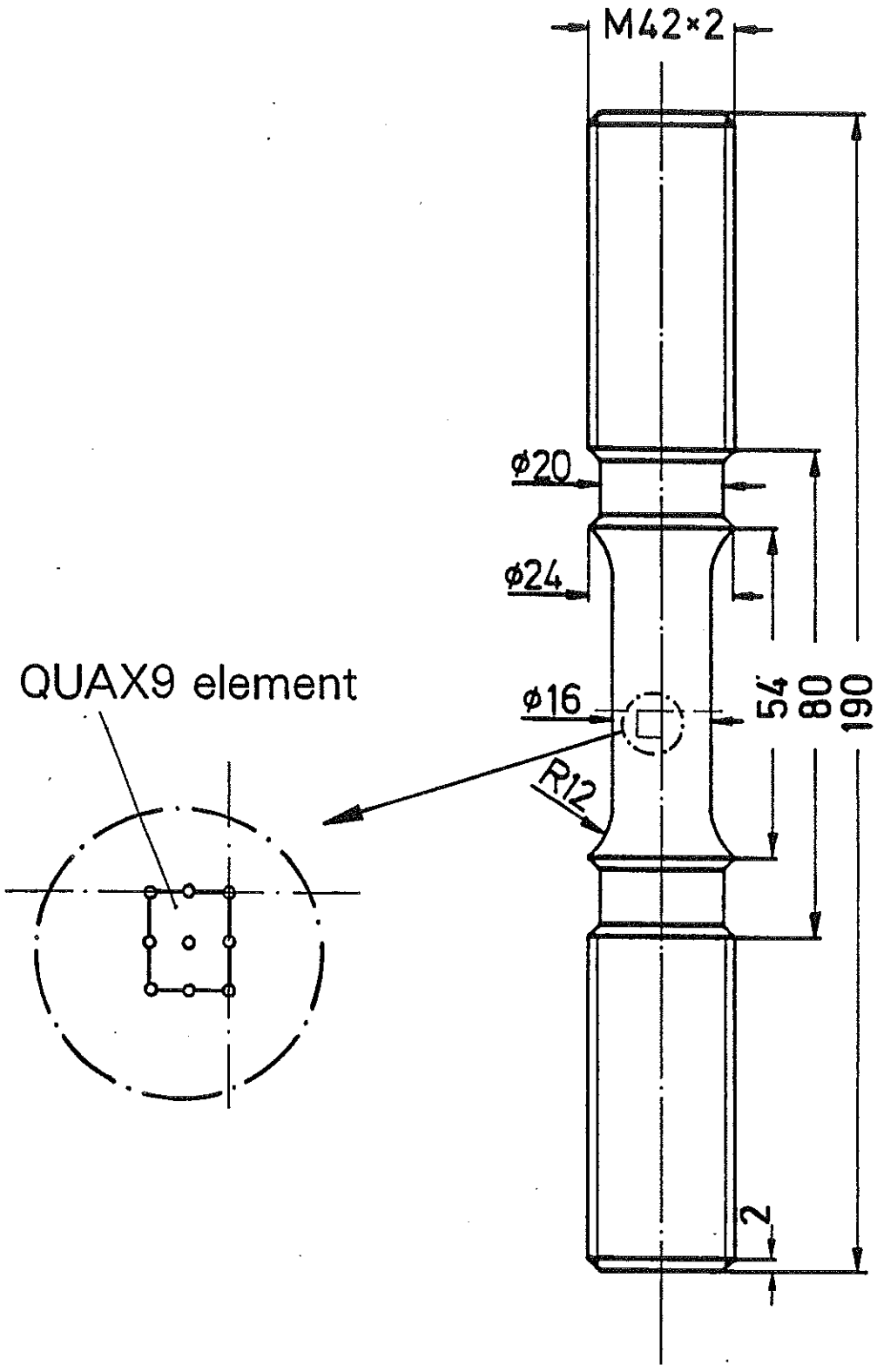

Fig. 8: Specimen for uniaxial cyclic loading

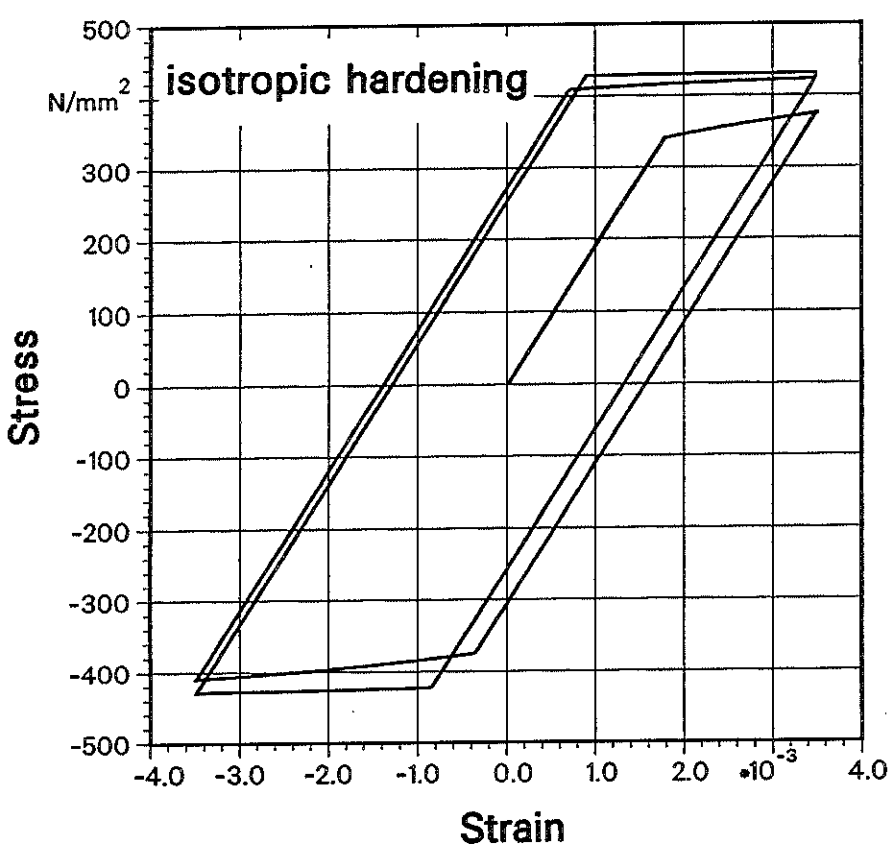

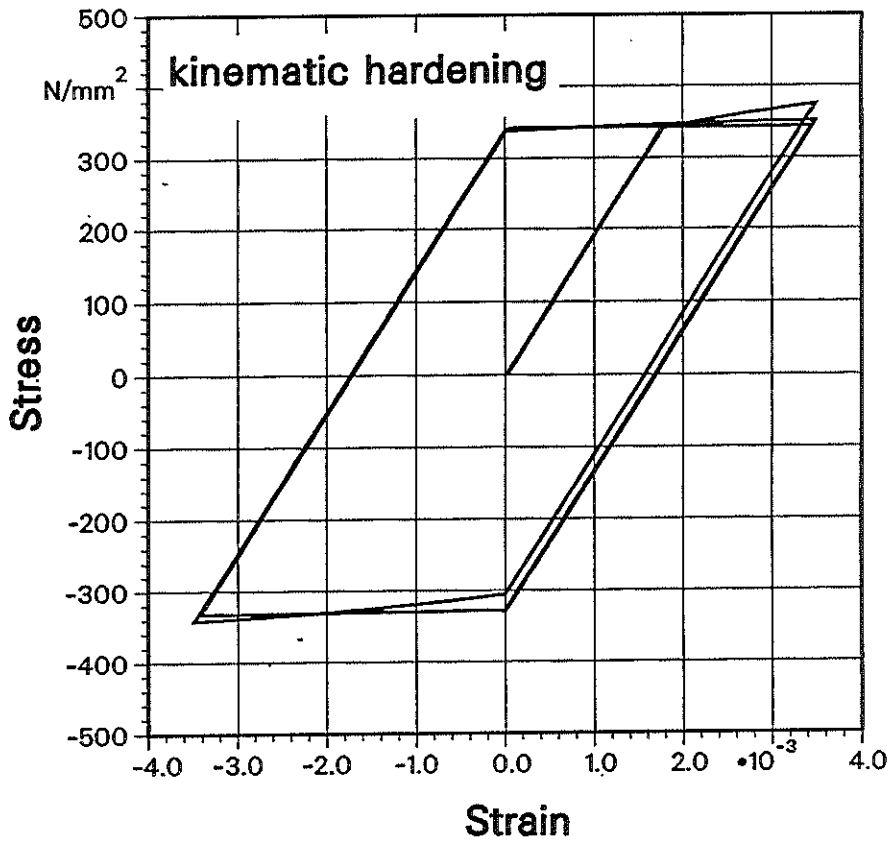

Fig. 9: Computed cyclic stress-strain curves

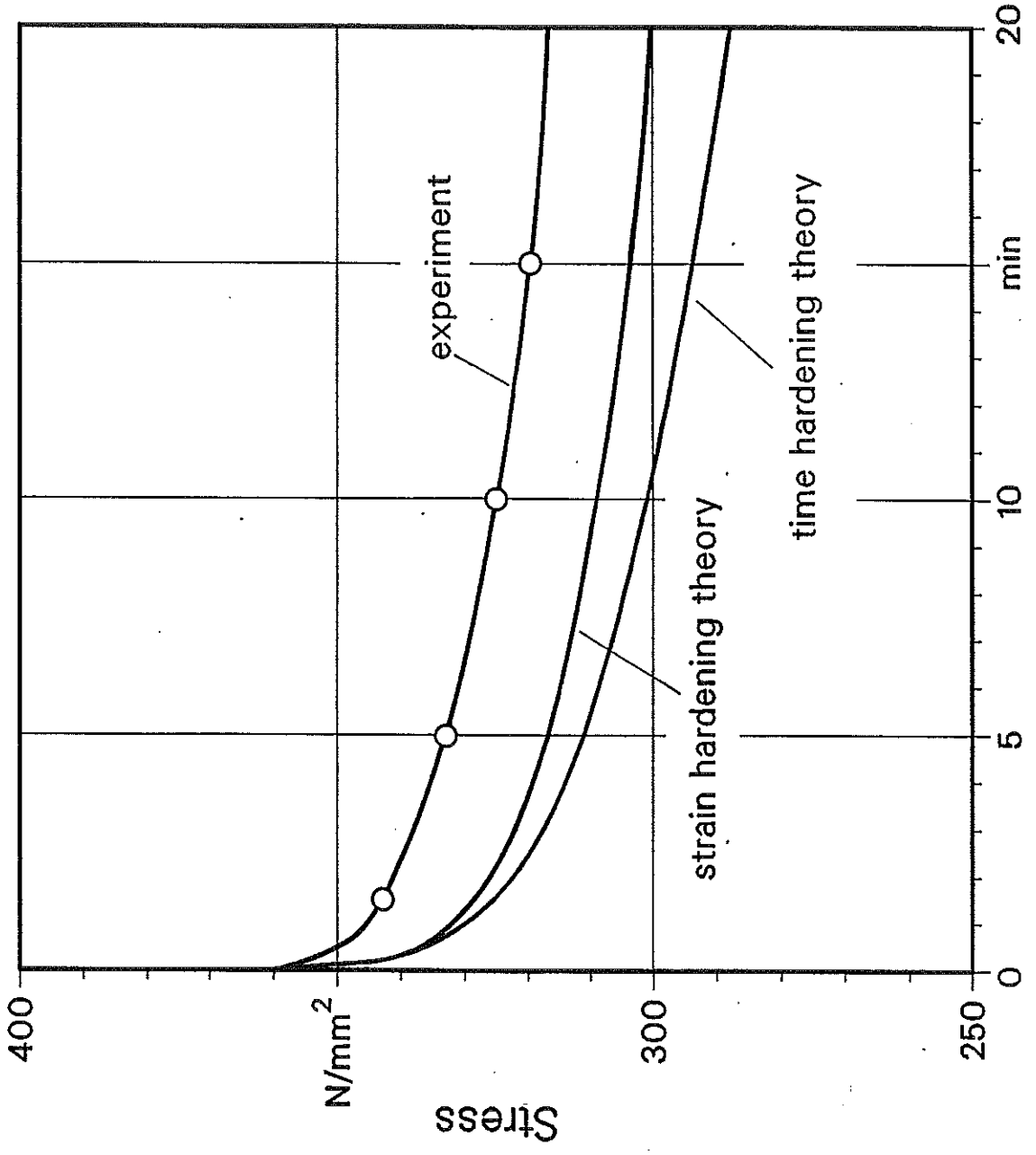

Fig. 10: Stress relaxation and comparison with experimental data

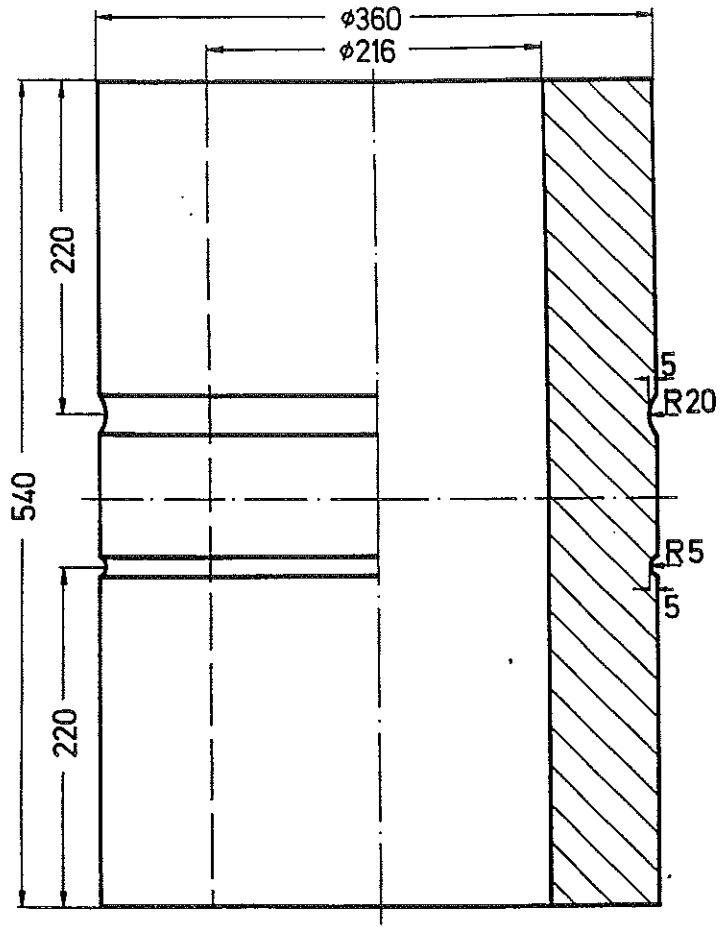

Fig. 11: Large scale specimen with main dimensions

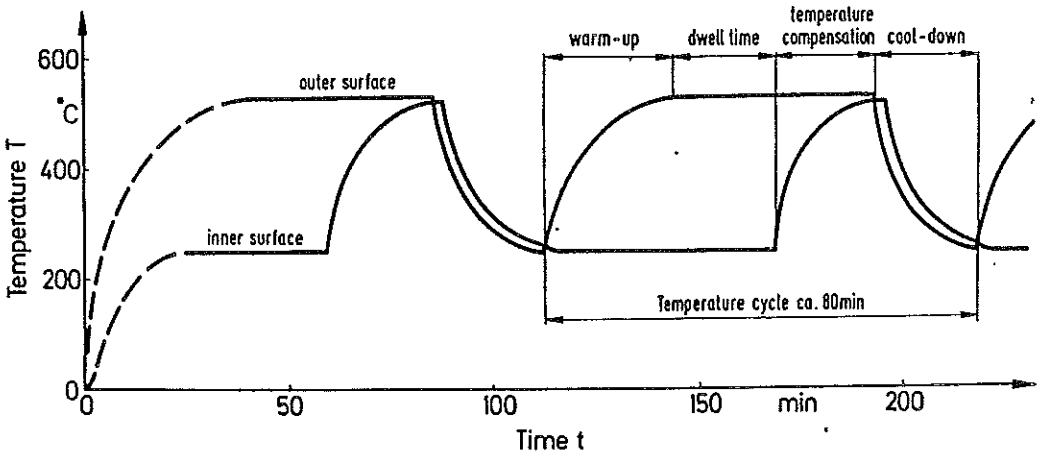

Fig. 12: Schematic temperature cycle, based on the actual temperature characteristics of a turbine shaft

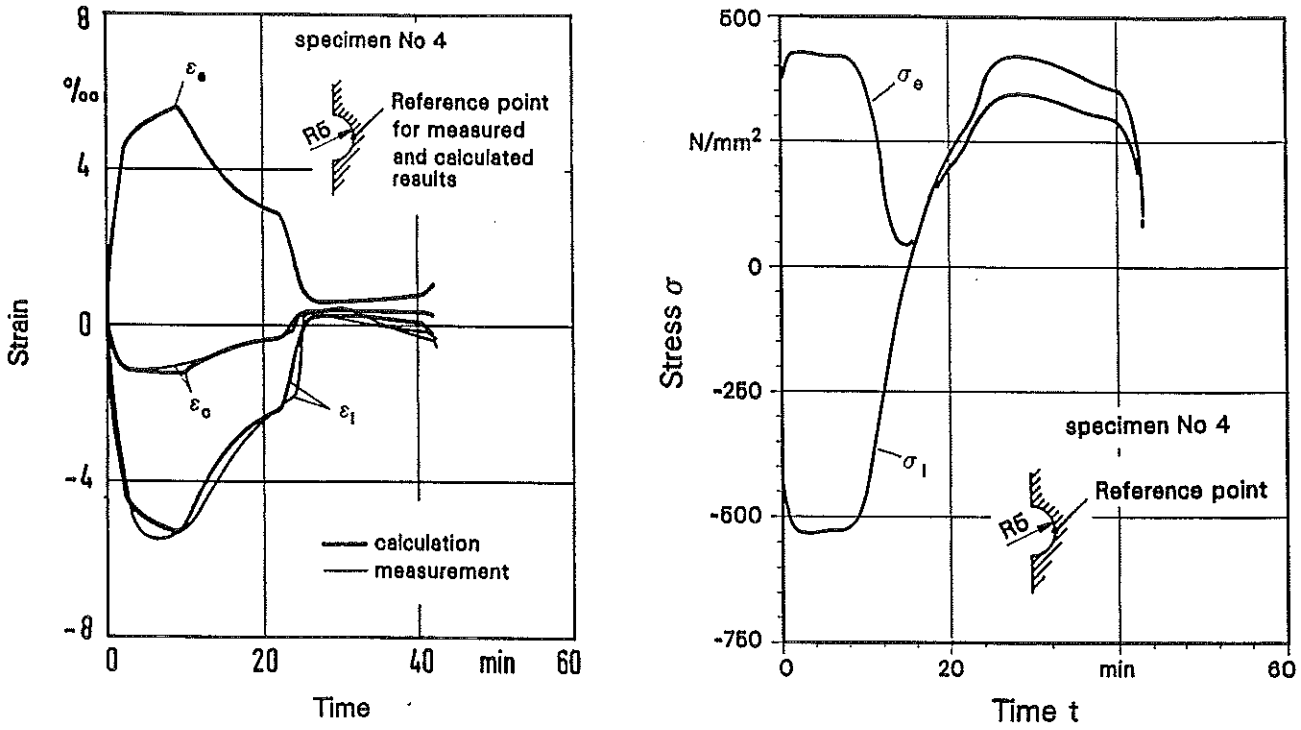

Fig. 13: Stresses and strains in the notched bottom
(c ≙ circumferential, l ≙ longitudional)

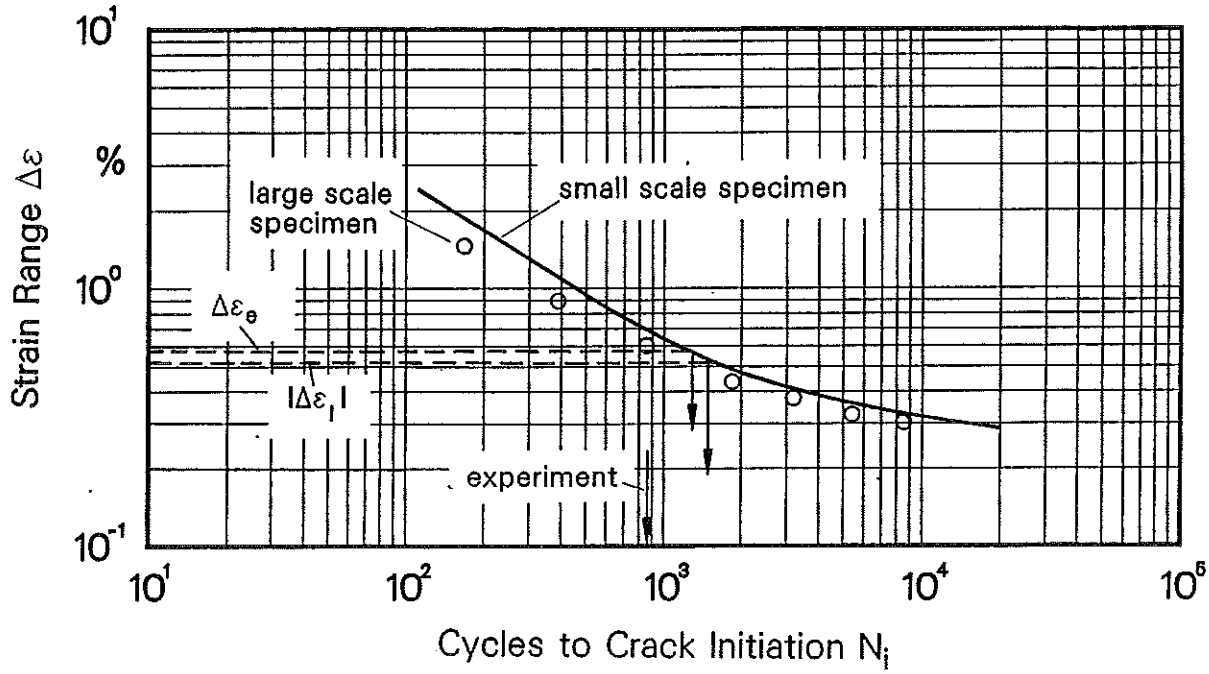

Fig. 14: Estimation of numbers of cycles to crack initiation

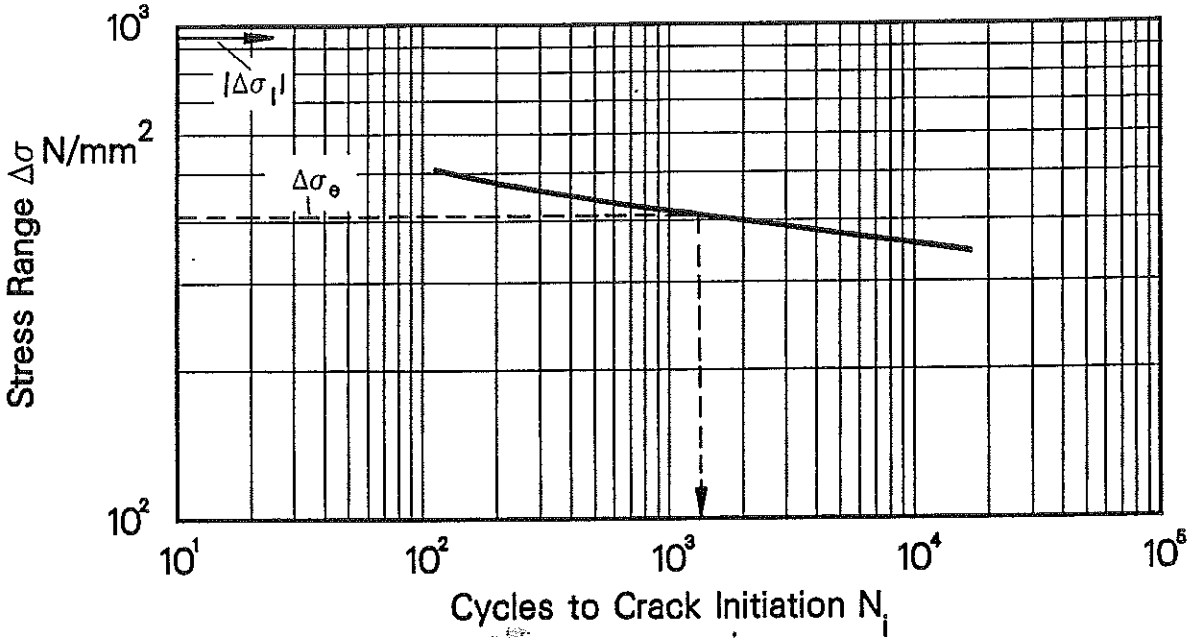

Fig. 15: Estimation of numbers of cycles to crack initiation on base of stress range for the crack initiation curve

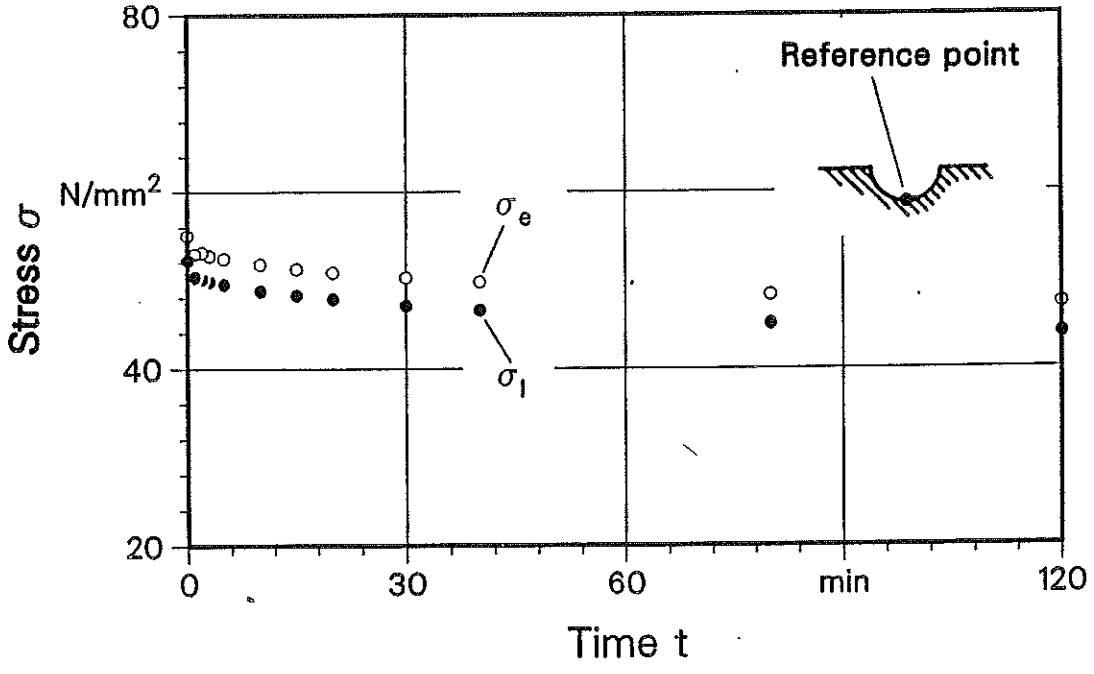

Fig. 16: Stress relaxation due to a dwell time of 120 min at constant temperature of 530 °C